Supporting Information

Ultra-Thin Composite Carbon Molecular Sieve Membranes from a Polymer of Intrinsic Microporosity Precursor

Wojciech Ogieglo*[$], Andreas Furchner[#], Xiaohua Ma[$], Khalid Hazazi[$], Abdulrahman T. Alhazmi[$], Ingo Pinnau*[$]

[$]*Functional Polymer Membranes Group, Advanced Membranes and Porous Materials Center, King Abdullah University of Science and Technology (KAUST), Thuwal 23955, Kingdom of Saudi Arabia*

[#]*Leibniz-Institut für Analytische Wissenschaften – ISAS – e.V., Schwarzschildstraße 8, 12489 Berlin, Germany*

Corresponding authors: wojciech.ogieglo@kaust.edu.sa; ingo.pinnau@kaust.edu.sa

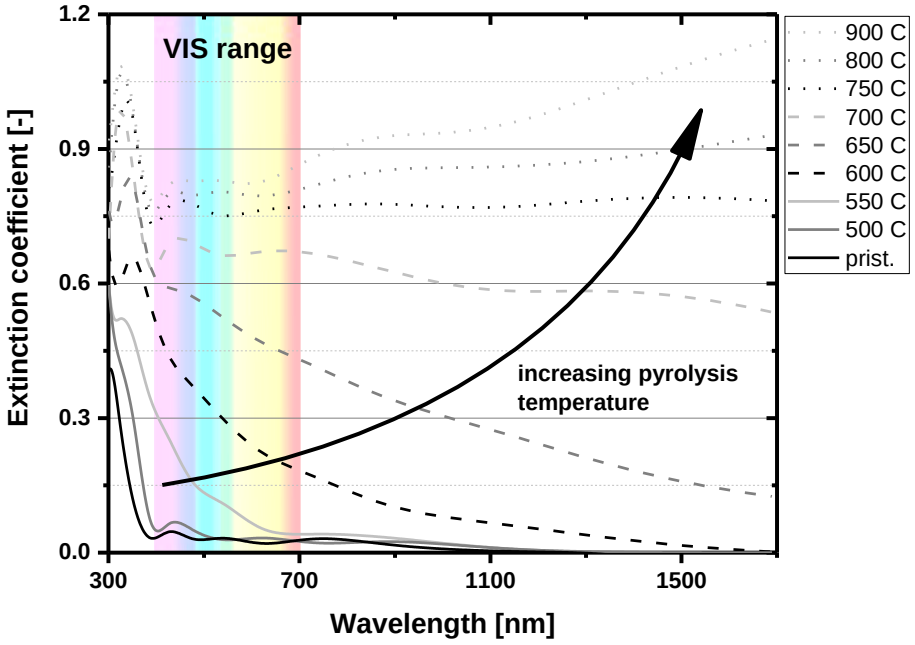

Figure S1. Broad wavelength range extinction coefficient of carbon films made from the ~300 nm thick PIM polyimide precursor extracted using the B-Spline parametrization of the dielectric function. The fitting was performed by first fitting the transparent part of the precursor film by a Cauchy model, wavelength expansion by 0.5 eV intervals down to 300 nm, and subsequent refitting with Kramers-Kronig consistent e1-e2 B-Splines (separated by 0.3 eV in photon energy); subsequently, the fitting procedure was repeated for incrementally increasing pyrolysis temperatures using the previous result as a new starting point. The procedure was found to yield numerically robust and physically realistic dielectric functions.

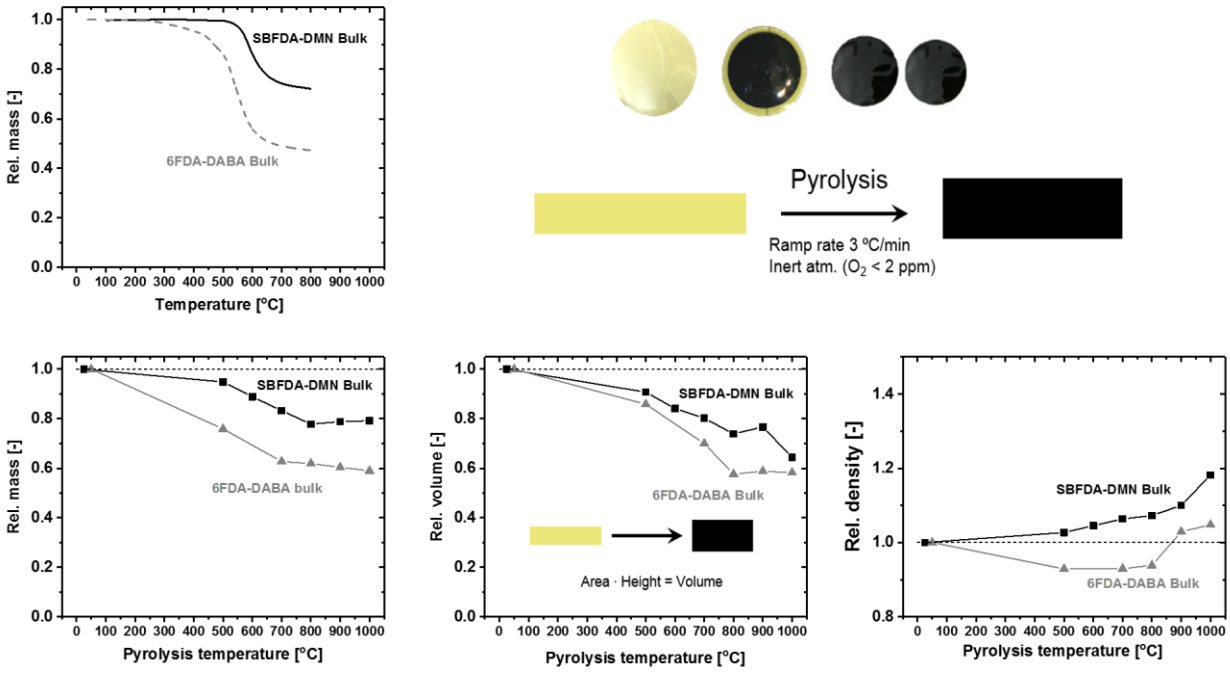

Figure S2. Powder TGA-derived weight loss and the relative volume, relative mass and relative density plotted against the pyrolysis temperature for bulk (thick films) of the PIM and non-PIM polyimides.

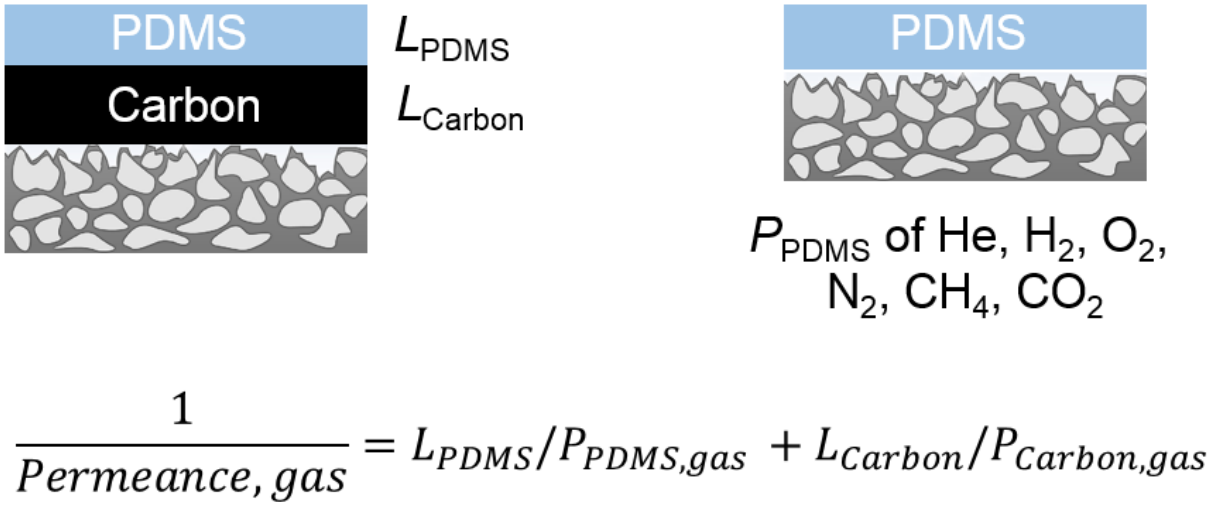

Figure S3. Resistance-in-series calculations used to extract the permeability of the carbon film for a particular gas ($P_{Carbon,gas}$) by combining the thicknesses of the respective layers determined with ellipsometry (L_{PDMS}, L_{Carbon}) and the separately measured permeability of PDMS alone deposited on the Anodisc® substrate.

Table S1 Properties of the PDMS Measured Separately as a Thin Film (~600 nm, averages of two separate samples) Deposited Directly on Top of the Anodisc® Substrate from Isooctane and Crosslinked for 2 Hours at 50 °C.

Permeability [Barrer]						Selectivity [-]	
He	H_2	N_2	O_2	CH_4	CO_2	O_2/N_2	CO_2/CH_4
269	470	186	417	622	2389	2.24	3.84

Table S2 Results of Anisotropic Optical Modeling Using IRSE of the Pristine and Pyrolyzed Films Deposited on Native Oxide Silicon Wafer Stated at the High-Frequency End of the Spectrum (4000 cm^{-1} and 8000 cm^{-1} compared with UV-VIS at 1000 nm).

	UV-VIS		IR (8000 cm^{-1})			IR (4000 cm^{-1})			
Sample	n_xy	n_z	n_xy	n_z	Error	n_xy	n_z	Error	Comment
Pristine	1.63041	1.61967	1.637	1.629	0.002	1.633	1.625	0.002	-
500 °C	1.65532	1.62966	1.672	1.670	0.005	1.667	1.665	0.005	-
550 °C	1.77378	1.70400	1.754	1.710	0.008	1.751	1.708	0.008	-
600 °C	2.01914	1.90496	1.945	1.848	0.015	1.888	1.787	0.015	-
650 °C	2.51566	2.15659	-	-	-	-	-	-	Film absorbing in NIR, too inhomogenous
700 °C	2.65225	1.95119	2.269	1.767	-	2.595	2.032	0.20	Film absorbing in NIR but almost homogenous

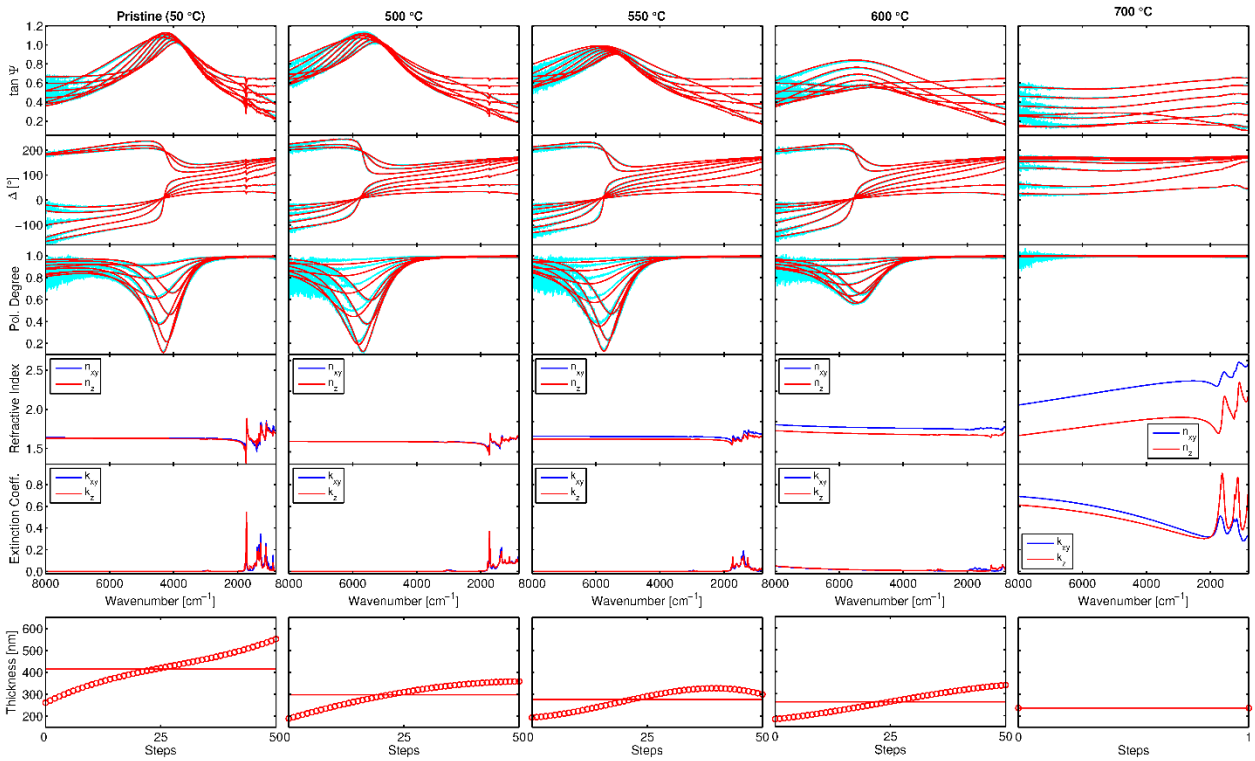

Figure S4. IRSE modeling results for some of the analyzed samples supplementing data from Table S1.

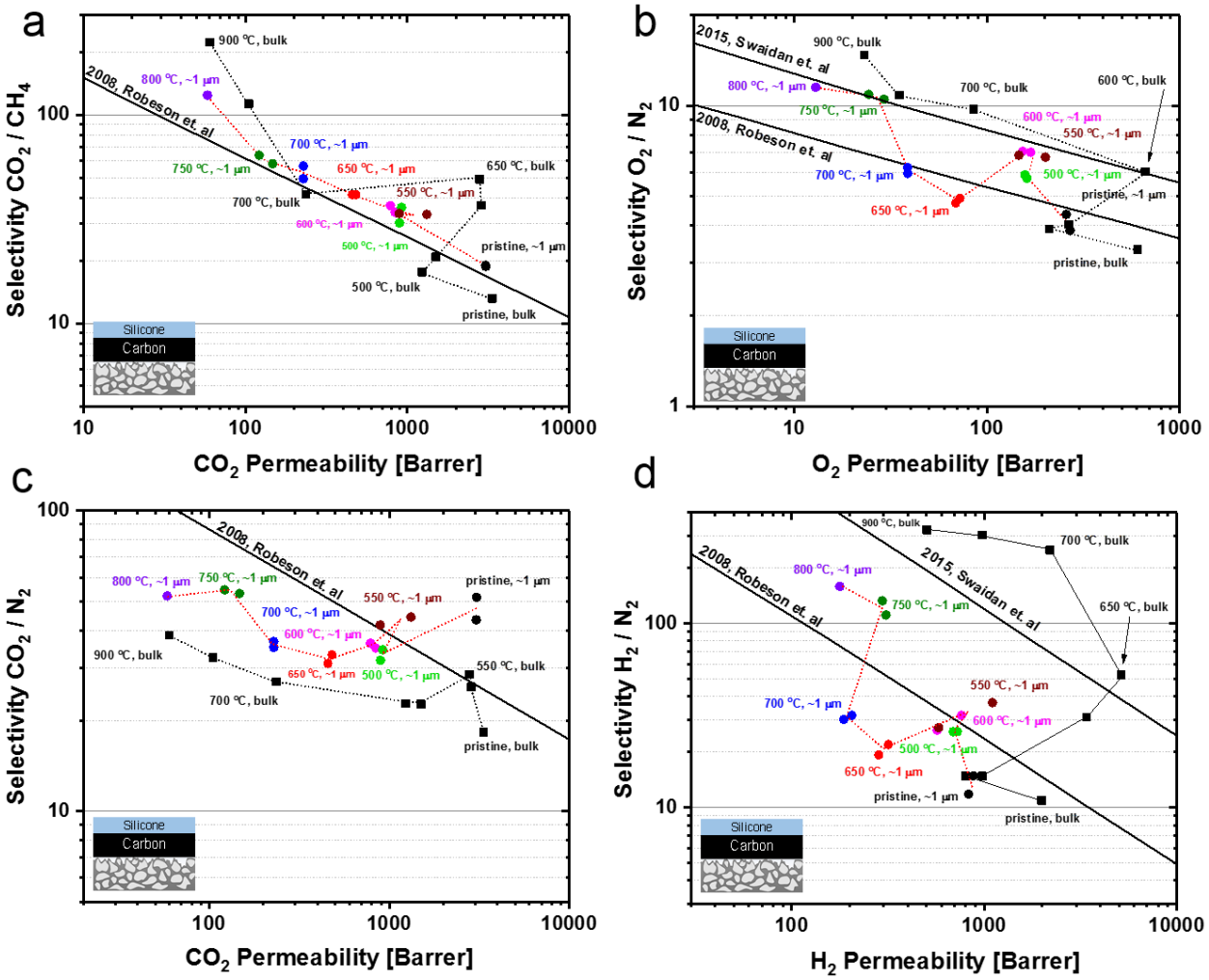

Figure S5. Trade-off diagrams for: a) CO_2/CH_4, b) O_2/N_2, c) CO_2/N_2, and d) H_2/N_2 for the bulk and ~1 micron PIM-derived carbon membranes. Each point represents average of two membrane samples measured separately. Error bars are omitted for clarity of presentation. The difference in the performance between the two separate samples was always below 15-20%.

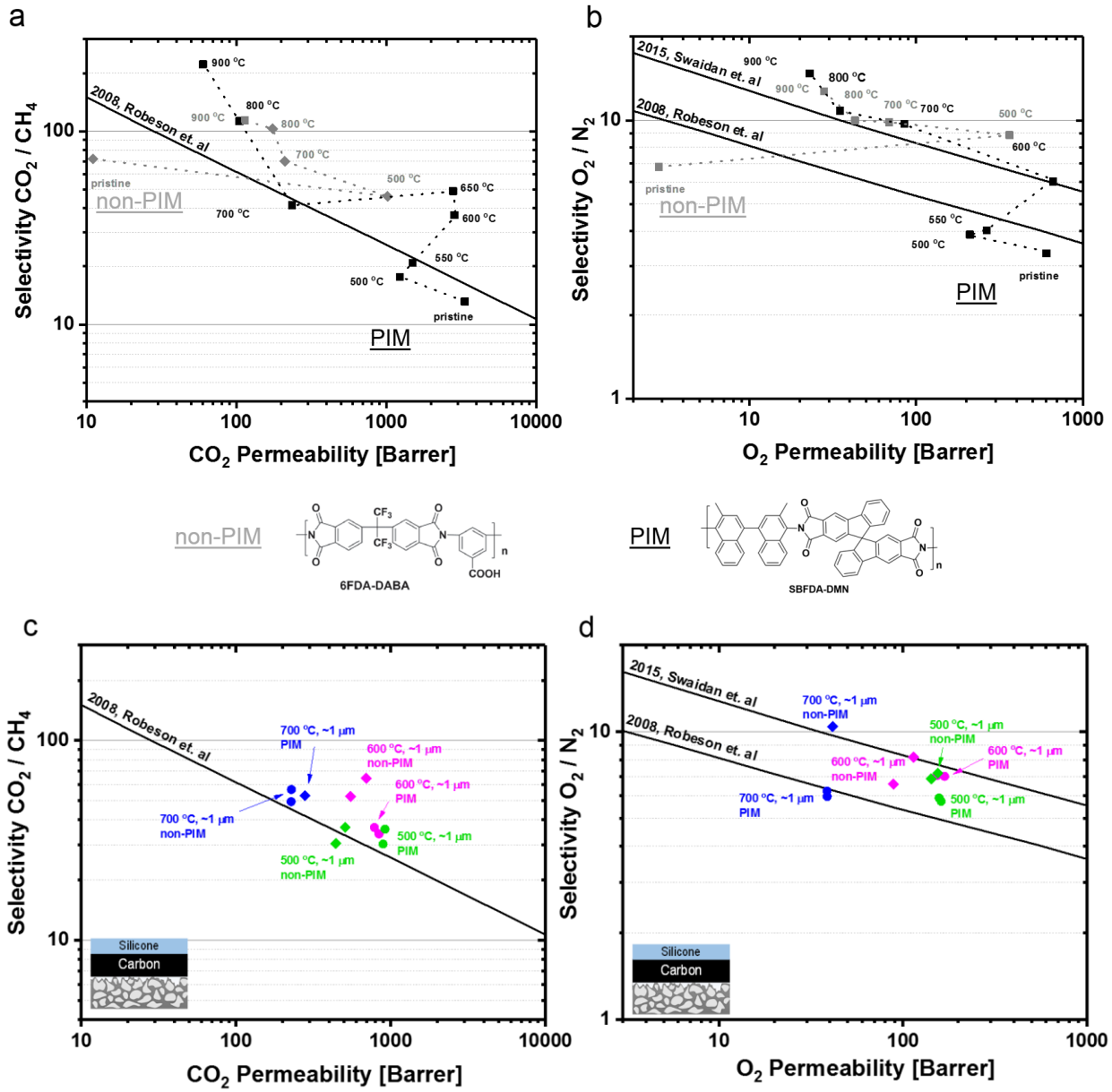

Figure S6. Separation performance expressed as CO_2/CH_4 and O_2/N_2 tradeoff diagrams for bulk (a, b) and thin (c, d) PIM and non-PIM carbons performance data.

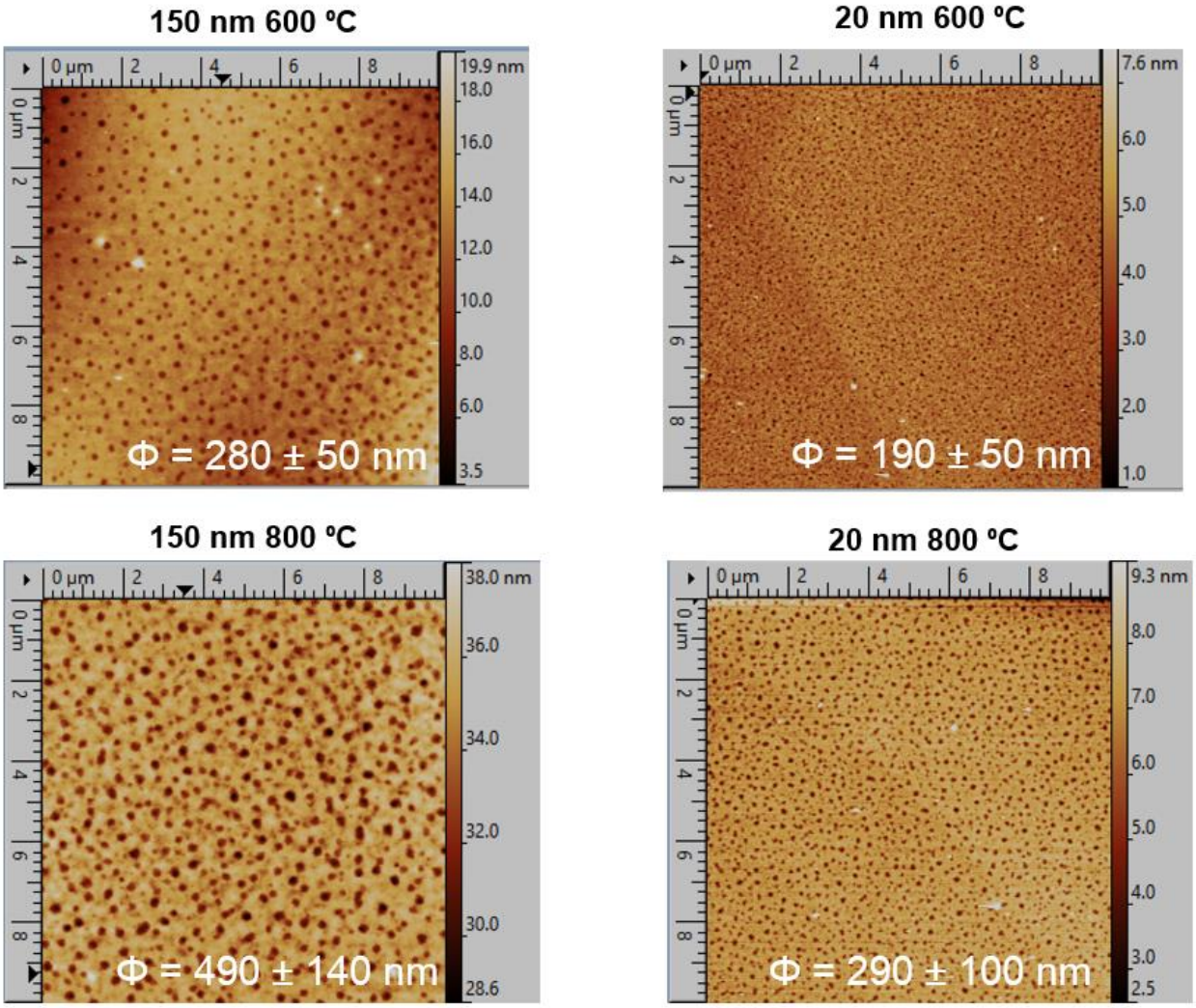

Figure S7. AFM tapping-mode surface topology maps of the PIM-derived surfaces for the 150 and 20 nm films pyrolyzed at 600 and 800 °C directly on top of a silicon wafer; development of large (relative to film thickness) 190 – 490 nm defects or pores is clearly seen.

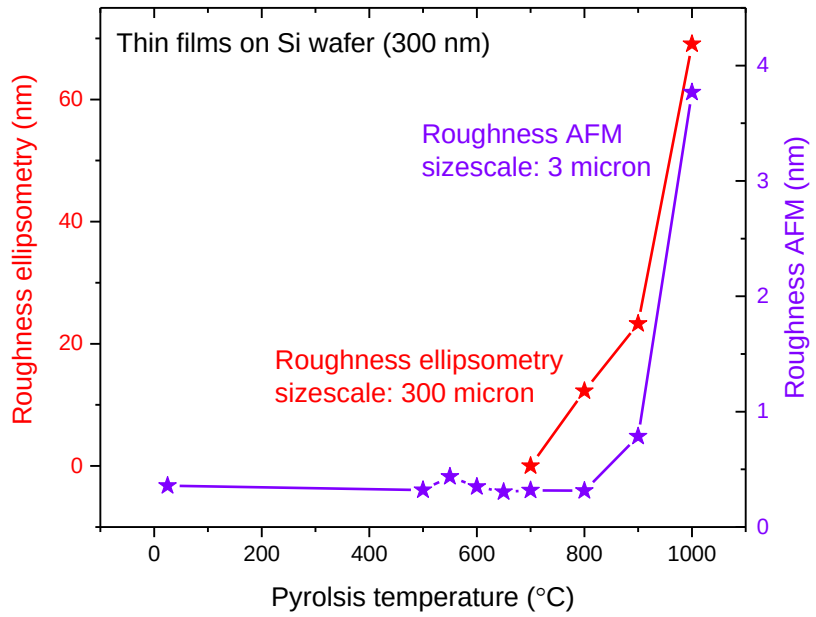

Figure S8. Ellipsometry- and AFM-derived roughness of the thin pristine and carbon films deposited on 500 nm Si oxide covered wafers.

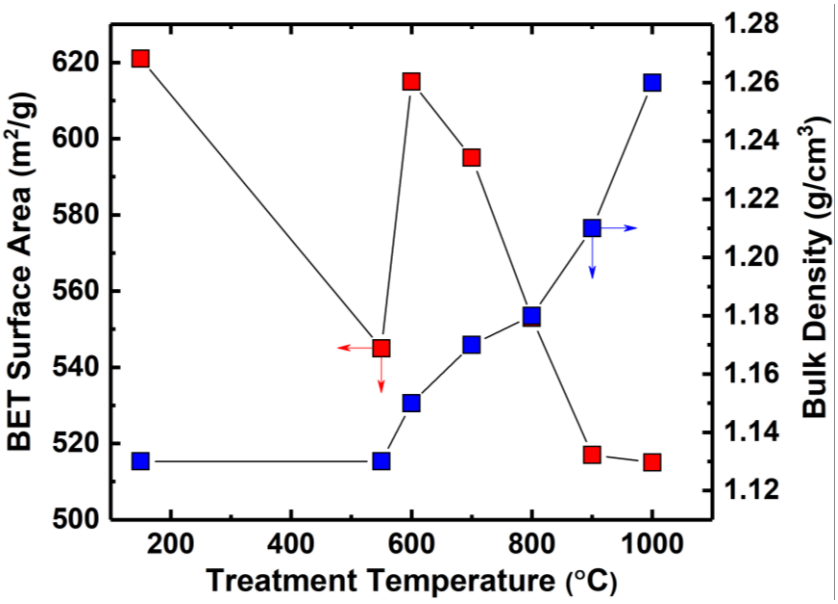

Figure S9. BET surface area and density for the bulk CMS samples made from the same SBFDA-DMN precursor as used for thin film CMS composite membranes. Reproduced from: Hazazi K. et al. submitted to Journal of Membrane Science 2019.

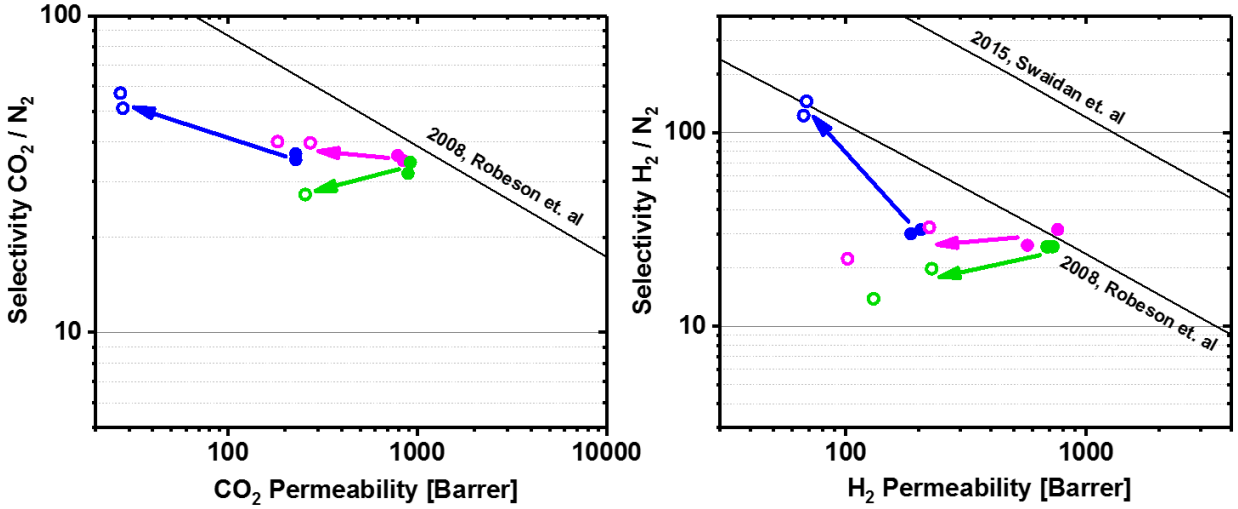

Figure S10. Performance of the thick (filled symbols) and thin (open symbols) fresh membranes benchmarked against Robeson trade-offs.

X-Ray Photoelectron Spectroscopy (XPS) analysis

The XPS experiments were performed on a Kratos Axis Ultra DLD instrument equipped with a monochromatic Al Kα x-ray source (hν = 1486.6 eV) operated at a power of 120 W and under UHV conditions in the range of ~ 10^{-9} mbar. All spectra were recorded in hybrid mode using electrostatic and magnetic lenses and an aperture slot of 300 µm × 700 µm. The survey and high-resolution spectra were acquired at fixed analyzer pass energies of 160 eV and 20 eV, respectively. The samples were mounted in floating mode in order to avoid differential charging and XPS spectra were thus acquired under charge neutralization condition.

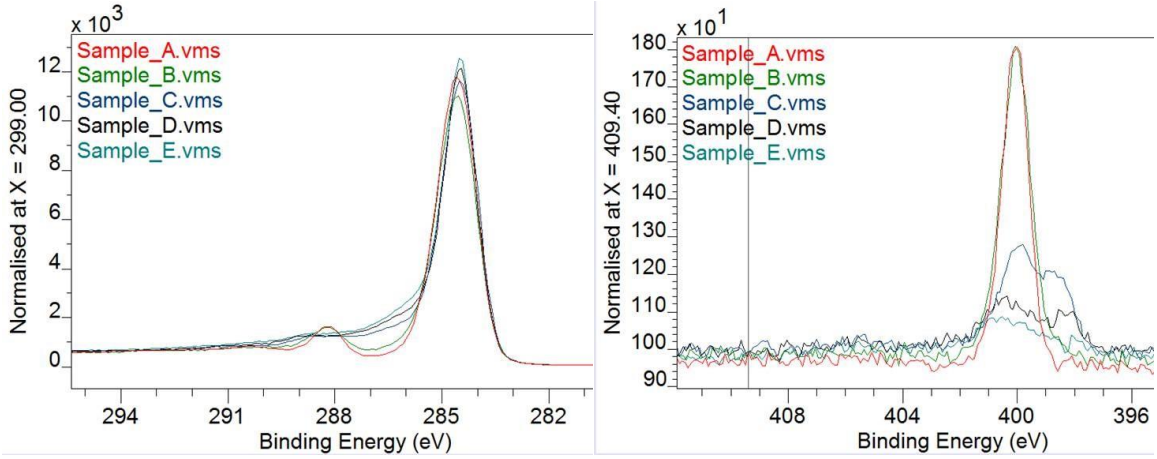

Figure S11. Performance of the thick (filled symbols) and thin (open symbols) fresh membranes benchmarked against Robeson trade-offs

Table S3. Elemental Composition of the Pristine and CMS Membrane Samples as Determined by XPS.

Sample	C [%]	N [%]	O [%]	F [%]	Si [%]	Cl [%]
Pristine	91.3	2.3	5.6	0.4	0.3	0.1
500 °C	89.7	2.3	7.8	-	0.1	0.1
600 °C	88.9	1.6	9.2	0.2	-	0.1
700 °C	91.5	1.0	7.5	-	-	-
800 °C	91.7	0.7	7.6	-	-	-